Fission and Fusion at the End of the Periodic System

Peter Möller, Arnold J. Sierk, Takatoshi Ichikawa and Akira Iwamoto

[1] *Theoretical Division, Los Alamos National Laboratory, Los Alamos, NM 87544*
[2] *Tokai Research Establishment, Japan Atomic Energy Research Institute(JAERI) Tokai-mura, Naka-gun, Ibaraki, 319-11 Japan*

We calculate in a macroscopic-microscopic model fission potential-energy surfaces for neutron-rich actinides and fission-fusion potential-energy surfaces relevant to the analysis of heavy-ion reactions employed to form heavy-element evaporation residues. We study the latter multidimensional potential-energy surfaces both inside and outside the touching point.

Inside the point of contact we define the potential on a multi-million-point grid in 5D deformation space where elongation, merging projectile and target spheroidal shapes, neck radius and projectile/target mass asymmetry are independent shape variables. The same deformation space and the corresponding potential-energy surface also describe the shape evolution from the nuclear ground-state to separating fragments in fission, and the fast-fission trajectories in incomplete fusion.

For separated nuclei we study the macroscopic-microscopic potential energy, that is the "collision surface" between a spheroidally deformed target and a spheroidally deformed projectile as a function of three coordinates which are: the relative location of the projectile center-of-mass with respect to the target center-of-mass and the spheroidal deformations of the target and the projectile. We limit our study to the most favorable relative positions of target and projectile, namely that the symmetry axes of the target and projectile are collinear.

We also calculate fission barriers for a long sequence of uranium isotopes. The aim is to understand another attempted production mechanism for superheavy elements, namely neutron-capture in thermonuclear explosions.

§1. Introduction

It has been a longstanding challenge to understand in detail element formation at the end of the periodic system. In nature many of the heaviest elements are formed in the rapid-neutron-capture process, r-process, in stars.[1)] About 20 elements beyond those present in significant quantities on earth have been artificially synthesized in laboratories, predominantly by use of heavy-ion reactions.[2)] We present here initial results of very large-scale fission-barrier calculations for neutron-rich nuclei relevant to nucleosynthesis at the end of the r-process and fusion-fission potential energy surfaces relevant to the artificial production of the very heaviest elements in cold-fusion reactions. About 25 years ago it became clear that rather than use the most asymmetric target and projectile combinations to extend the periodic system further, so called cold-fusion reactions with a target near ^{208}Pb were preferable.[3)] This double magicity confers extra binding energy to the colliding system. This has no effect on the barrier between the colliding heavy ions relative to infinite separation, but it does lower the barrier relative to the ground-state of the compound system.

Here we will identify what other aspects of cold-fusion reactions favor compound-nucleus formation, apart from the long-recognized benefit of the lower excitation energy. In particular we will look at the potential energy both before and after

typeset using $\mathcal{PTP}$TEX.cls ⟨Ver.0.89⟩

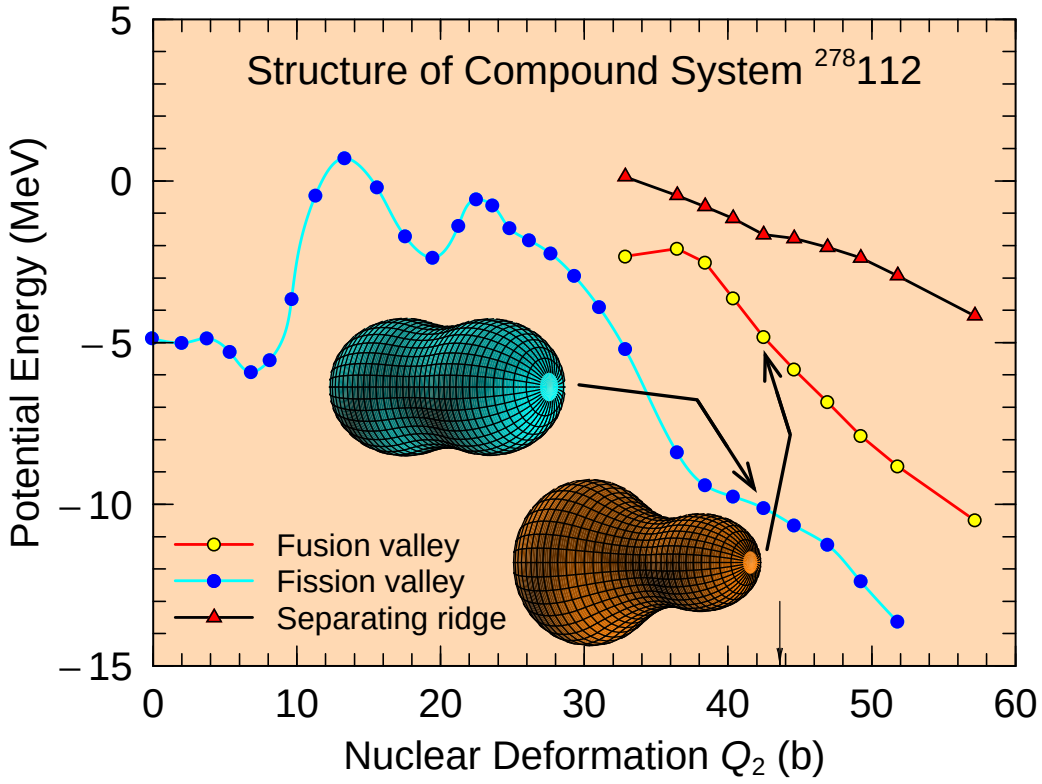

Fig. 1. Structures in the calculated 5D potential-energy surface of ^{278}112. The lower curve corresponds to the fission barrier. For large values of Q_2 there is an additional well-defined valley in the 5D energy surface, which is stabilized with respect to the fission valley by the ridge shown in the top curve. One shape in the fission valley and one shape in the additional valley are shown. The shape in the additional valley corresponds to $M_{\rm H}/M_{\rm L} = 208/70$. The position of the vertical thin arrow on the horizontal axis indicates the value of Q_2 at the contact point for *spherical* target and projectile.

touching in a multidimensional deformation space in a model that takes microscopic effects into account, and see how this picture differs from a purely macroscopic picture.

§2. Five-dimensional compound-system potential-energy surfaces

The five-dimensional macroscopic-microscopic potential-energy surfaces for compound systems reached in cold-fusion heavy-ion reactions are calculated and analyzed using the same techniques as introduced previously in studies of actinide fission.[4] In particular we calculate the potential energy as a function of 5 nuclear-shape coordinates: 15 points each in the neck diameter and left and right fragment deformations, 35 points in the mass asymmetry, and 33 points in the nuclear elongation. This leads to a space of 3898125 grid points. However, as explained elsewhere[4] some grid-point coordinate values do not correspond to physically realizable shapes;

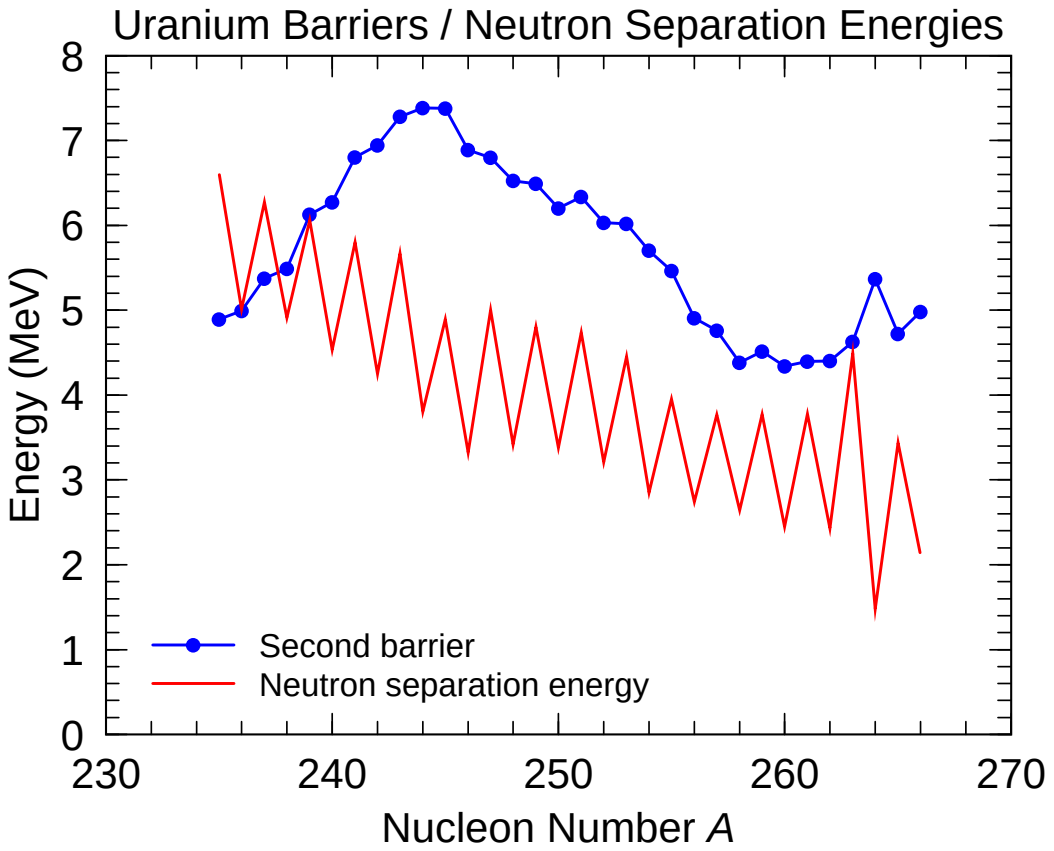

Fig. 2. Calculated outer fission-barrier heights for a sequence of uranium isotopes. Also shown is the neutron separation energy for the $A+1$ system. When the separation energy is higher than the fission barrier fission is possible when a neutron is captured during the r-process.

therefore the actual number of grid points considered are 3594915. Compared to our previous fission studies we have increased the number of mass-asymmetry grid points from 20 to 35.

In Fig. 1 we show the result of a water-immersion analysis of the calculated 5D deformation spaces for the compound system $^{278}112$. The shapes in the secondary valley strongly overlap with the target and projectile masses in the incident channel. This appearance of the potential-energy surface is very different from what is obtained in a macroscopic multi-dimensional picture in which these systems just after touching find themselves on a surface that slopes steeply sideways relative to the incident direction and therefore would immediately deflect systems colliding "at the Coulomb barrier" towards the fission valley and re-separation.[5)–7)]

In Fig. 2 we show for a sequence of uranium isotopes the calculated value of the *outer* peak in the barrier. In the vicinity of $A = 260$ the calculated outer barrier height is less than 5 MeV. In a 3D calculation in a deformation grid appropriate for studies of the first peak in the fission barrier we find that its height is also below 5 MeV. Thus the r-process could be terminated here by neutron-induced fission.

However, for a more complete description it is necessary to calculate barriers for the entire neutron-rich heavy-element region and follow β-decay to stability and determine the associated β-delayed neutron-emission and β-delayed fission branching ratios. These studies are in progress. However, we can already note that in thermonuclear explosions designed to generate particularly high neutron fluences only nuclei with mass number A up to $A = 257$ were produced with uranium targets.[8] This is in qualitative agreement with Fig. 2, where the calculated neutron separation energies become close to the calculated barrier heights just below $A = 260$.

§3. Three-dimensional heavy-ion collision potential-energy surfaces

We study here the fusion barrier for some cold-fusion reactions commonly used to reach heavy elements in the region from No to proton number $Z = 114$.

It is well known that the "Coulomb barrier" calculated in simple macroscopic models with spherical targets and projectiles is much higher than the optimal energy for forming heavy evaporation residues in heavy-ion collisions. We therefore use a more realistic approach and calculate below the energy of a colliding heavy-ion system as

$$\begin{aligned} E_{\mathrm{P+T}}(\epsilon_{2\mathrm{P}}, \epsilon_{2\mathrm{T}}, x_{\mathrm{P}}, y_{\mathrm{P}}, z_{\mathrm{P}}, \alpha, \beta, \gamma) = {} & E^{\mathrm{self}}_{\mathrm{P}}(\epsilon_{2\mathrm{P}}) - E^{\mathrm{self}}_{\mathrm{P}}(\epsilon_{2\mathrm{P}} = \mathrm{gs}) \\ & + E^{\mathrm{self}}_{\mathrm{T}}(\epsilon_{2\mathrm{T}}) - E^{\mathrm{self}}_{\mathrm{T}}(\epsilon_{2\mathrm{T}} = \mathrm{gs}) \\ & + E^{\mathrm{int}}_{\mathrm{PT}}(\epsilon_{2\mathrm{P}}, \epsilon_{2\mathrm{T}}, x_{\mathrm{P}}, y_{\mathrm{P}}, z_{\mathrm{P}}, \alpha, \beta, \gamma) \qquad (3{\cdot}1) \end{aligned}$$

Here $E_{\mathrm{P+T}}$ is the total energy of the colliding system relative to infinitely separated targets and projectiles in their ground states (gs). The quantity E^{self} is the macroscopic-microscopic potential energy as a function of shape as given by our FRLDM model.[4),9)] Since we give the system energy *relative* to the separated fragments we obviously need to subtract the ground-state self-energies of the target and projectile; thus the second and fourth terms in the right member of Eq. 3·1 above. The interaction-energy-term calculation is extensively discussed in our Ref.[10)] We assume that the interaction shell-correction energy can be neglected for separated target and projectile. The Cartesian triplet $(x_{\mathrm{P}}, y_{\mathrm{P}}, z_{\mathrm{P}})$ gives the location of the center of the projectile relative to the center of the target. The Euler angles α, β, and γ specify the orientation of the projectile symmetry axis relative to the target symmetry axis. The energetically most favorable configuration, at least for prolate deformations, for a specific distance between target and projectile, is when the axes of the target and projectile are collinear. To limit the problem to a moderately low-dimensional parameter space we therefore only consider these relative positions of target and projectile and only spheroidal deformations $\epsilon_{2\mathrm{T}}$ and $\epsilon_{2\mathrm{P}}$ of the target and projectile, respectively. Thus, we have $x_{\mathrm{P}} = 0, y_{\mathrm{P}} = 0, \alpha = 0, \beta = 0$, and $\gamma = 0$, so that the space we investigate is 3-dimensional and is characterized by target and projectile spheroidal deformations and their relative distance z_{P}. The configuration we consider is also referred to as the polar-parallel configuration.[11)]

We now argue that if the system loses stability with respect to target and/or projectile deformation as the ions approach each other then the energy at which this

Table I. Heavy-ion-reaction fusion barriers calculated in three models. The first model (a) is the conventional Coulomb barrier. In the second model (b) projectile deformation and target and projectile microscopic corrections are included. In the third model (c) the variation in zero-point energy with respect to the projectile spheroidal deformation as the projectile approaches the target is also considered. We have verified that the effect of target deformation is very small, only an MeV or so in most cases, due to the stabilizing effect of the doubly-magic proton and neutron numbers $Z = 82$ and $N = 126$ of the target.

Reaction	1-D Coul. Barr. (a) (MeV)	2-D Saddle (b) (MeV)	2-D Saddle (c) (MeV)
$^{48}_{20}$Ca + $^{208}_{82}$Pb → $^{258}_{102}$No	182.65	179.04	178.70
$^{50}_{22}$Ti + $^{208}_{82}$Pb → $^{258}_{104}$Rf	201.04	194.29	193.87
$^{54}_{24}$Cr + $^{208}_{82}$Pb → $^{262}_{106}$Sg	218.44	209.93	208.60
$^{58}_{26}$Fe + $^{208}_{82}$Pb → $^{266}_{108}$Hs	236.13	224.97	221.96
$^{62}_{28}$Ni + $^{208}_{82}$Pb → $^{270}_{110}$Ds	252.71	244.21	239.04
$^{64}_{28}$Ni + $^{208}_{82}$Pb → $^{272}_{110}$Ds	251.48	238.43	238.58
$^{70}_{30}$Zn + $^{208}_{82}$Pb → ^{278}112	267.14	255.05	252.26
$^{74}_{32}$Ge + $^{208}_{82}$Pb → ^{282}114	284.49	280.07	271.71
$^{76}_{32}$Ge + $^{208}_{82}$Pb → ^{284}114	283.85	275.09	272.40

occurs defines a more realistic fusion-barrier height. This means that we assume that once the system becomes unstable with respect to deformation, shape changes occur very fast relative to motion in the collision direction. Specifically we determine for a succession of values of $z_{\rm P}$ the minimum energy with respect to target and projectile deformation and the corresponding target and projectile deformations. If we neglect the microscopic terms in $E^{\rm self}$ we recover the well-known result that the target and projectile are fairly oblate: ϵ_2 is in the range -0.4 to -0.2 in the situations investigated. However, when the microscopic corrections are included they stabilize the doubly magic ^{208}Pb at spherical or very close to spherical shape; deviations are typically less than 0.03. We can therefore illustrate the important aspects of the collision surface in only two dimensions. In Figs. 3 and 4 we show the energy of the colliding system for a spherical target versus projectile deformation for a succession of distances as the projectile approaches the target for two heavy-ion reactions leading to $^{258}_{104}$Rf and ^{278}112. We indicate by a big blob the energy corresponding to the "conventional" Coulomb barrier calculated as the maximum in the macroscopic energy between spherical target and projectile. For the light compound system the Coulomb barrier is only 5.57 MeV higher than the energy at the point where our more realistic collision surface loses stability with respect to projectile deformation. The situation is quite different for the heavy compound system ^{278}112. Here the collision-surface saddle point is 14.09 MeV lower than the Coulomb barrier. In Table 1 we present calculations of the collision-surface saddle-point energy for 11 heavy-ion collisions in the second column of numbers. These have been calculated assuming the target is spherical. We have also relaxed this

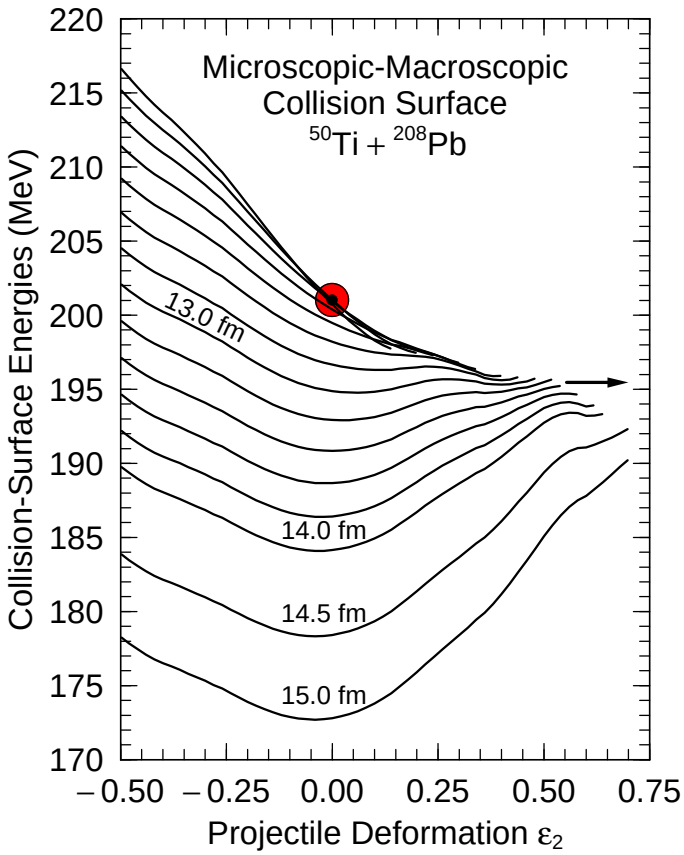

Fig. 3. Calculated macroscopic-microscopic potential energies for the collision of ^{50}Ti+^{208}Pb. Each of the plotted curves shows the potential energy of the system versus projectile deformation, for spherical ^{208}Pb and a specific distance between the centers of mass of the target and projectile. The distance in fermi, is written above the potential-energy curve. For distances less than 14.0 fm the separation between projectile and target decreases by 0.2 fm for each successive curve. The dot corresponds to the calculated value of the one-dimensional "Coulomb barrier" in a macroscopic model. The arrow indicates the fusion-barrier height obtained by the method corresponding to column 3 in Table 1. It is plotted at an energy that is slightly different from the energy in the table to be "consistent" with the curves in the figure, see text for a discussion.

condition but for a ^{208}Pb target the effect on the barrier is usually less than 1 MeV. For comparison we also present, in column one, the conventional Coulomb barrier.

The potential energy curves in Figs. 3 and 4 have all been calculated assuming that target and projectile zero-point energies do not change as the ions approach. However when projectile stability with respect to deformation is lost the projectile zero-point energy vanishes. The correct fusion barrier in this approximation (column 2 in Table 1) is therefore obtained by subtracting the projectile zero-point energy at infinity from the saddles obtained from the energies in this figure. For the case when we calculate the point of instability by taking into account the changing projectile zero-point energy (column 3 in Table 1) we also subtract this zero-point energy and

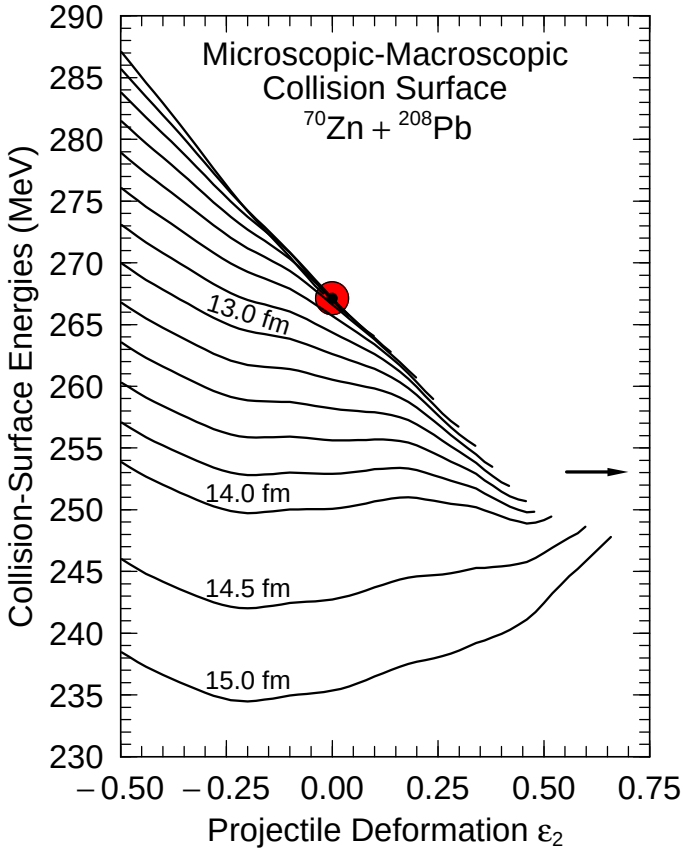

Fig. 4. Same as Fig. 3, but for the collision ^{70}Zn+^{208}Pb. Here the difference between the conventional Coulomb barrier and the collision-surface saddle-point height is substantial.

add the appropriate projectile zero-point energy at the current separation. The arrow energies in Figures 3 and 4 are "consistent" with the energy curves, that is the projectile zero-point energies at infinite separation have not been subtracted out. They are therefore located at slightly different energies than the fusion barrier energies listed in Table 1 which are normalized so that they are consistent with experimental energies given in the center-of-mass frame.

In Fig. 4 we observe that the energy curves versus projectile deformation are very flat for a succession of distances before stability with respect to projectile deformation is lost. Therefore the exact energy and deformation where this occurs depends somewhat on the procedure used to find the minimum energy with respect to projectile and target deformation at each separation and on other minor details of the calculations. We therefore consider an improved model for determining the collision-surface saddle point.

We consider the target to be inert, that is, based on the observations above, we keep its shape spherical. For each separation we then calculate the zero-point energy with respect to projectile deformation. That is we calculate the zero-point

energies for each of the one-dimensional curves shown in Figs. 3–5. The curves are approximated by parabolas whose minima coincide with the actual function minima and pass through the saddle towards prolate projectile deformations (or when a saddle is non-existent pass through the maxima at the touching point). For the inertia with respect to ϵ vibrations we use exactly the same model as we have used to calculate the ground-state zero-point energies in our mass model[12] and in fission half-life calculations.[13] When the sum of the zero-point energy and the minimum energy of the curve is equal to the saddle energy towards the right in Figs. 3 and 4 we claim we have found the collision-surface saddle point. We only calculate the zero-point energy for a set of curves at separation distances ... 14.0, 13.8, 13.6, 13.4 ... and then determine by interpolation the point where the zero-point energy coincides with the saddle occurring towards the right on the curves. The collision-surface saddle-point energies determined in this way are given in the third column of numbers in Table 1. We have also calculated the zero-point energies with a WKB method. The collision-surface saddle-point energy obtained by WKB differs from the value obtained in the parabolic approximation by less than 0.1 MeV on the average, despite the non-parabolic appearance of many of the curves in Figs. 3 and 4.

In Fig. 5 we plot the collision-surface saddle relative to the ground-state energy of the compound system. We compare this realistic model of the fusion barrier to two models of the Coulomb barrier. The "Total fusion" takes into account the effect of microscopic corrections on the nuclear masses, whereas "Macroscopic fusion" does not. The "total-fusion" macroscopic-microscopic barrier is considerably lower than the macroscopic barrier, relative to the ground state of the compound system. However, relative to the separated projectile and target configuration the two barriers are equally high. This is the well-known "cold-fusion" effect: The total fusion barrier relative to the ground state of the compound system is lowered due to the extra binding associated with the doubly-magic nucleus ^{208}Pb. Other contributions, which can be positive or negative, arise from the microscopic corrections in the projectile and evaporation residue nuclei. Thus, in a cold fusion reaction "at the Coulomb barrier" the compound system will form at lower excitation energies than in non-cold-fusion reactions leading to the same system. This effect is thought to enhance the evaporation-residue cross section.

We also plot the fission barriers of the compound systems. They are compared to the ground-state microscopic corrections. The "Enhancement to binding" curve shows the ground-state microscopic correction multiplied by -1, to make it more obviously comparable to the fission-barrier height. Since the macroscopic fission barrier is almost non-existent for these systems, the fission-barrier height will be roughly equal to the (negative of the) ground-state microscopic correction.[14),15)] Of interest here is that the calculated fusion-barrier height drops down to about the fission-barrier height at around compound-system proton number $Z = 112$. This means that for higher proton number it is roughly the fission-barrier peak that is the highest point on the fusion path. We initially discussed this at the ENAM98 conference, Fig. 3 in that paper.[16] (However, the fusion-barrier calculations there are inaccurate due to incorrect coding of the Wigner-term shape dependence.) An important consequence is that when the fusion-barrier height drops down to the

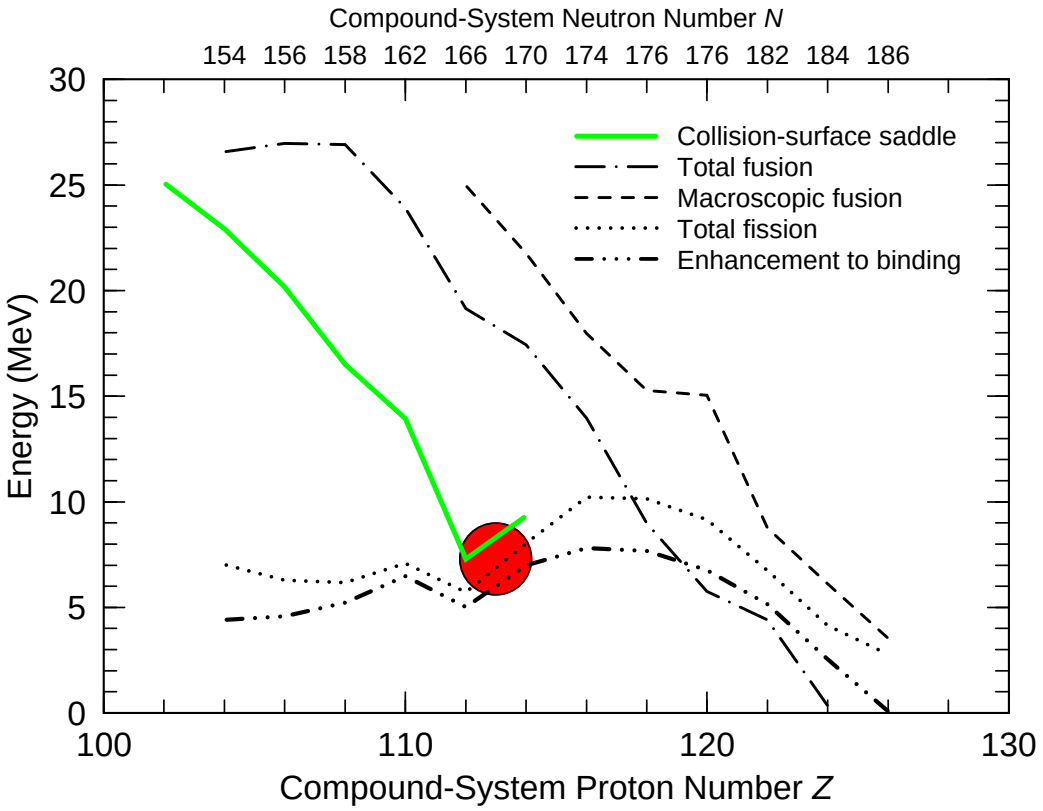

Fig. 5. Potential-energy-surface barrier and ground-state systematics for cold-fusion reactions leading to compound systems from No to $Z = 126$. The "Enhancement to binding" curve is exactly the ground-state microscopic correction multiplied by -1. Curves labeled "Total" are calculated with the full macroscopic-microscopic approach. However, both the "Macroscopic fusion" and "Total fusion" results were obtained assuming that target and projectile are spherical during the collision. The "Collision-surface saddle" curve was calculated permitting projectile deformation; otherwise the model is identical to "Total Fusion". See text for further discussions.

fission barrier, one must expect a break in the systematics for the optimum energy for evaporation residue formation that is now, for unknown systems typically obtained from the trend of this energy extrapolated from lighter systems.

§4. Conclusions

Traditionally in dynamical models of colliding heavy ions the potential energy has been described in terms of a macroscopic model. Deformations of target and projectile are sometimes also ignored. We have shown here that for collisions at low energy, that is "at the Coulomb barrier" deformations and microscopic effects contribute to a dramatically different picture of the potential energy.

Inside the touching point we find a substantial "cold-fusion" valley where the shape configuration corresponds closely to the shape of target and projectile just before touching, that is an almost spherical target-like part joined with a deformed

projectile part, with a deformation similar to what develops just before touching.

Outside the touching point our more realistic model shows that in collisions leading to very heavy systems, for example $^{272}112$ the collision-surface saddle point where stability with respect to projectile deformation is lost is about 14 MeV lower in energy than the conventional Coulomb barrier. This gives a more reasonable correspondence between calculated fusion-barrier heights, which we now equate with the collision-surface saddle-point energy, and the observed most-favorable energies for evaporation residue formation.

Clearly there is a need to go further to understand more completely the mechanism of evaporation-residue formation. Just as shape and microscopic corrections bring major changes to our picture of the static aspects of heavy-ion collisions leading to very heavy systems, there is also a need to consider these in modeling other quantities, for example the inertia and the dissipation mechanisms associated with the collision, and when compound-nucleus formation has occurred the various de-excitation mechanisms need to be described. However, we hope our more realistic modeling of some static aspects of heavy-ion collisions will lead to productive steps also in these directions.

An alternative heavy-element production method is neutron capture in thermonuclear explosions. We have shown above that our calculated barriers and neutron-separation energies for a long sequence of uranium isotopes is roughly consistent with the result that no nuclei heavier than $A = 257$ were observed in explosions with uranium targets. However, a more complete understanding of the isotope production in these events require further analysis.

This research is supported by the US DOE.

References

1) K.-L. Kratz, J.-P. Bitouzet, F.-K. Thielemann, P. Möller, and B. Pfeiffer, Astrophys. J. **403** (1993) 216.
2) S. Hofmann, F. P. Hessberger, D. Ackermann, G. Münzenberg, S. Antalic, P. Cagarda, B. Kindler, J. Kojouharova, M. Leino, B. Lommel, R. Mann, A.G. Popeko, S. Reshitko, S. Śaro, J. Uusitalo, A.V. Yeremin, Eur. Phys. J. A **14**, (2002) 147.
3) P. Armbruster, Compt. Rend. Phys. **4** (2003) 571.
4) P. Möller, D. G. Madland, A. J. Sierk, and A. Iwamoto, Nature **409** (2001) 785.
5) J. R. Nix and A. J. Sierk, Phys. Scr. **10A** (1974) 94.
6) P. Möller and J. R. Nix, Nucl. Phys. **A272** (1976) 502.
7) P. Möller and A. J. Sierk, Nature, **422** (2003) 485.
8) S. A. Becker, Carnegie Observatories Astrophysics Series, Vol 4, Origin and Evolution of the Elements, 2003, ed. A. McWilliam and M. Rauch (Pasadena: Carnegie Observatories, http://www.ociw.edu/ociw/symposia/series/symposium4/proceedings.html).
9) P. Möller, J. R. Nix, W. D. Myers, and W. J. Swiatecki, Atomic Data Nucl. Data Tables **59** (1995) 185.
10) P. Möller and A. Iwamoto, Nucl. Phys. **A575** (1994) 381.
11) A. Iwamoto, P. Möller, J. R. Nix, and H. Sagawa, Nucl. Phys. **A596** (1996) 329.
12) P. Möller and J. R. Nix, Nucl. Phys. **A361** (1981) 117.
13) P. Möller and J. R. Nix, Phys. Rev. Lett. **37** (1976) 1461.
14) W. J. Swiatecki, Phys. Rev. **100** (1955) 937.
15) Z. Patyk, A. Sobiczewski, P. Armbruster and K.-H. Schmidt, Nucl. Phys. **A491** (1989) 267.
16) P. Möller, Proc. ENAM 98, Exotic Nuclei and Atomic Masses, Bellaire, Michigan, 23–27 June, 1998 (AIP Conference Proceedings, **455** (1998) 698).